Formation of droplets and bubbles in a microfluidic T-junction—scaling and mechanism of break-up†

Piotr Garstecki,*[ab] Michael J. Fuerstman,[a] Howard A. Stone[c] and George M. Whitesides*[a]

Received 29th July 2005, Accepted 5th January 2006
First published as an Advance Article on the web 25th January 2006
DOI: 10.1039/b510841a

This article describes the process of formation of droplets and bubbles in microfluidic T-junction geometries. At low capillary numbers break-up is not dominated by shear stresses: experimental results support the assertion that the dominant contribution to the dynamics of break-up arises from the pressure drop across the emerging droplet or bubble. This pressure drop results from the high resistance to flow of the continuous (carrier) fluid in the thin films that separate the droplet from the walls of the microchannel when the droplet fills almost the entire cross-section of the channel. A simple scaling relation, based on this assertion, predicts the size of droplets and bubbles produced in the T-junctions over a range of rates of flow of the two immiscible phases, the viscosity of the continuous phase, the interfacial tension, and the geometrical dimensions of the device.

1. Introduction

There is a growing interest in microfluidic techniques for highly controlled formation of droplets[1–12] and bubbles.[13–18] One of the most frequently used microfluidic geometries to produce immiscible fluid segments is a T-junction.[3,5,8,19,20] In spite of the popularity of the T-junction geometry, neither the process of break-up, nor a quantitative analysis of the sizes of the droplets it produces, have been detailed, and only partial observations are available.[3,21] Here we study the process, scaling characteristics, and mechanism of break-up of liquid and gas streams in T-junctions over a wide range of rates of flow and viscosities of the fluids. The class of the T-junction geometries that we tested is representative of those used in analytical microfluidics. In particular, we focused on planar geometries, with rectangular cross-sections of the channels, in which (i) the width of the main channel is similar or greater than its height, and (ii) the inlet channel is comparable in width to the main channel.

We find that at low values of the capillary number—when the interfacial forces dominate the shear stresses—the dynamics of break-up of immiscible threads in T-junctions is dominated by the pressure drop across the droplet or bubble as it forms. In this *squeezing* regime the process of break-up is similar to the rate-of-flow-controlled break-up that we described previously[16] for flow-focusing geometries, and the size of the droplets or bubbles is determined solely by the ratio of the volumetric rates of flow of the two immiscible fluids. This characteristic leads to a simple scaling law for the size of the discrete fluid segments:

$$L/w = 1 + \alpha Q_{in}/Q_{out} \quad (1)$$

where L is the length of the immiscible slug, w is the width of the channel, $Q_{in/out}$ are the rates of flow of the dispersed and carrier fluids respectively, and α is a constant of order one, whose particular value depends on the geometry of the T-junction. The scaling relation (eqn (1)) is independent of the material parameters of the fluids—their viscosities and the interfacial tension between them. This effect is specific to microsystems: at rates of flow (10^{-2} to 1 μL s^{-1}) that are typically used for flow in microchannels (having characteristic dimensions on the order of 100 μm), the capillary numbers ($Ca = \mu u/\gamma$, where μ is the viscosity, and u is the mean speed of the carrier fluid, and γ is the interfacial tension) are typically small ($Ca < 10^{-2}$). As a result, the shear stresses exerted on the interface of the emerging droplet are not sufficient to distort it significantly. Consequently, the droplet (or bubble) blocks almost the entire cross-section of the main channel and confines the flow of the carrier fluid to thin wetting films on the walls of the microchannel. This leads to an increase of pressure upstream of the emerging droplet and leads to 'squeezing' of the neck of the immiscible thread. Squeezing proceeds at a rate proportional to the rate of flow of the carrier fluid, and sets the time for the growth of the droplet or bubble; this growth, in turn, proceeds at a rate proportional to the rate of flow of the dispersed phase. Collecting these two effects into a single equation yields the scaling relation described by eqn (1).

Importantly, as we observed experimentally and in numerical simulations[22] there is a critical value of the capillary number ($Ca_{CR} \sim 10^{-2}$) above which the shear stresses start to play an important role in the process of break-up, and the system starts to operate in a mode similar to the dripping regime in an unbounded, co-flowing liquid.[23,24] Here we focus

[a]*Department of Chemistry and Chemical Biology, Harvard University, 12 Oxford St., Cambridge, MA 02138, USA. E-mail: garst@ichf.edu.pl; gwhitesides@gmwgroup.harvard.edu*
[b]*Institute of Physical Chemistry, Polish Academy of Sciences, Kasprzaka 44/52, 01-224 Warsaw, Poland*
[c]*Division of Engineering and Applied Sciences, Harvard University, 29 Oxford St., Cambridge, MA 02138, USA*
† Electronic supplementary information (ESI) available: Liquid–liquid system (Fig. S1) and gas–liquid system (Fig. S2). See DOI: 10.1039/b510841a

on the squeezing regime, as it corresponds to values of rates of flow that are typical for those used in microfluidics. We verified the accuracy and range of applicability of the scaling relation (eqn (1)) experimentally by investigating the size of droplets and bubbles as a function of the (i) rate of flow and (ii) viscosity of the continuous fluid, (iii) the rate of flow, or the pressure applied to the discontinuous stream, (iv) the presence or absence of surface-active additives, and (v) the geometrical dimensions of the device. We detail the mechanism of break-up and the ranges of rates of flow, pressures, and material parameters (viscosity, interfacial tension) that promote stable, controllable formation of monodisperse liquid–liquid and gas–liquid emulsions in microfluidic devices.

Flow in microchannels

Flow of fluids in microfluidic systems are usually characterized by low values of the Reynolds number ($Re = \rho u l/\mu$, with ρ and μ being the density and dynamic viscosity of the fluid respectively, u the speed of flow, and l the characteristic dimension of the system). For $Re \ll 1$ flow is dominated by viscous stresses and pressure gradients—inertial effects are negligible—and the trajectories of fluidic particles can be controlled precisely.[25] This control[26] has led to a number of applications,[27] including, exposure of living cells to continuous[28] and step[29] changes of concentration of bio-active molecules or temperature, high-throughput screening,[30] and lab-on-chip immunoassays.[31]

Bubbles and drops in microfluidics

In recent years several groups have extended the use of microfluidic systems to multiphase flows with a special interest in formation of dispersions. Several techniques exist for formation of droplets[1–12] and bubbles.[13–18] These systems enable formation of dispersions with highly attractive features, particularly the control over the size and volume fraction of the dispersed phase,[3,6,14,15,32] and narrow distribution of the sizes of individual droplets or bubbles.[3,10,14,15] The use of immiscible fluids, and the controlled formation of microscale, individual fluid segments, both offer new routes to devices and systems that would perform chemical reactions and physico–chemical analyses on chip, using small volumes of reagents. Several tools for—and demonstrations of—microfluidic chemical processing based on droplets have already been demonstrated, including mixing,[5] controllable fusion and fission of droplets and bubbles,[33,34] crystallization of proteins,[35] synthesis of nanoparticles,[19] and bioassays.[36] Microfluidic dispersion-generators can also produce, in a highly controllable fashion, solid particles[37–41] and arrays of liquid crystalline droplets.[42]

The use of the T-junction geometry

Perhaps the most popular microfluidic device used for the generation of droplets is a T-junction geometry (Fig. 1), first incorporated into a microfluidic chip by Thorsen *et al.*,[3] and, subsequently used for formation of droplets[3,5] and bubbles,[19] for characterization of mixing in segmented liquid–liquid[5] and liquid–gas[19] flows, for formation of double emulsions[8] and in a host of analytical applications.[20,43–45] Most of these applications require precise control over the formation of the immiscible fluid segments. We have demonstrated control, and developed an analytical understanding, of the mechanism of break-up[16] for a flow-focusing system generating microbubbles at low values of the capillary number. Generation of liquid drops in a flow-focusing setup has also been demonstrated[4,10] and characterized.[46] Here we detail the process of break-up and the scaling of the size of the discrete fluid elements produced in the T-junction geometries over a range of typical values of rates of flow and viscosities of the fluids.

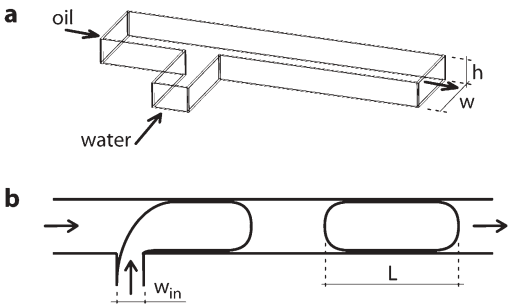

Fig. 1 (a) A schematic illustration of the microfluidic T-junction composed of rectangular channels. The channels are planar and have uniform height h. (b) A top view of the same schematic in a two-dimensional representation. Flow along the main channel proceeds from left to right. We flow the continuous fluid (here 'oil') along the main channel of width w, and we supply the fluid that will be dispersed (here 'water') *via* the orthogonal inlet of width w_{in}. In this work we consider geometries in which $1 \leqslant w/w_{in} \leqslant 4$. In inset (b) we schematically show the interface between the two immiscible fluids. We refer to the length L of the droplet as the distance between the furthest downstream and upstream points along the interface of a fully detached immiscible plug.

2. Results and discussion—liquid–liquid systems

The geometry of a T-junction

Fig. 1a and b illustrate schematically the geometry of a T-junction. Two channels merge at a right angle. The main channel carries the continuous (or 'carrier') fluid and the orthogonal channel (hereafter 'inlet channel') supplies the fluid that will be dispersed (hereafter 'dispersed' or 'discontinuous' fluid). The channels have rectangular cross-sections, and there are only three geometrical parameters that define the size and shape of the T-junction: the width w of the main channel, the width w_{in} of the channel supplying the discontinuous fluid and the height h of the channels.

Break-up in a T-junction

A typical process of formation of droplets (or bubbles) in the T-junction geometries that we studied can be described as follows. The two immiscible fluids form an interface at the junction of the inlet and main channel. The stream of the discontinuous phase penetrates into the main channel and a droplet begins to grow; the pressure gradient and the flow in the main channel distort the droplet in the downstream direction. The interface on the upstream side of the droplet

moves downstream. When the interface approaches the downstream edge of the inlet for the discontinuous phase, the neck connecting the inlet channel with the droplet breaks. The disconnected liquid plug flows downstream in the main channel, while the tip of the stream of the discontinuous phase retracts to the end of the inlet and the process repeats.

Over a wide range of rates of flow of both phases, this process generates uniformly sized droplets. The volume of these droplets can be adjusted by changing the rates of flow of the dispersed phase (here: Q_{water}) and the carrier fluid (Q_{oil}). Fig. 2a,b illustrates this dependence and shows several representative micrographs of the system at different values of Q_{oil} and Q_{water}. We are interested in how the sizes of the droplets formed in a T-junction depend on the rates of flow, the viscosity μ of the continuous fluid, the viscosity μ_d of the discontinuous fluid (not studied here), the interfacial tension γ between the two phases, and the geometrical dimensions of the device. In order to verify the influence of the geometrical parameters, we performed experiments in five different devices with dimensions listed in Table 1. In order to check the dependence of the size of the droplets on Q_{water}, Q_{oil}, μ, and γ we used the 'reference' geometry numbered '1' in Table 1 (h = 33 μm, w = 100 μm, w_{in} = 50 μm).

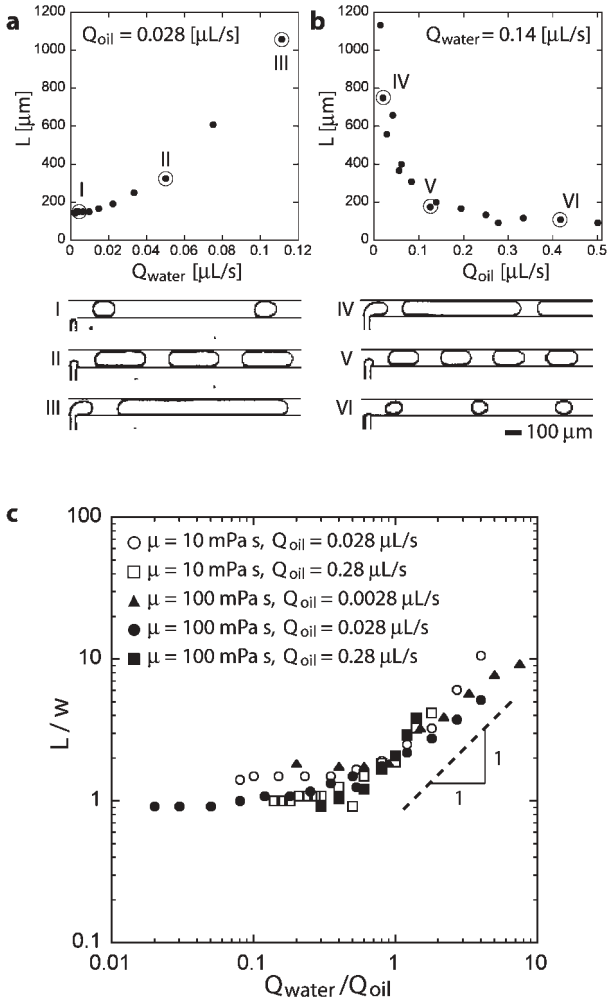

Fig. 2 Dependence of the length L of the aqueous droplets produced in the T-junction (h = 33 μm, w = 100 μm, w_{in} = 50 μm), on the rates of flow of the discontinuous (Q_{water}) and continuous (Q_{oil}) phases. (a) $L(Q_{water})$ for constant value of Q_{oil} = 0.028 μL s^{-1}, (b) $L(Q_{oil})$ for Q_{water} = 0.14 μL s^{-1}. The Roman numerals correspond to the optical micrographs shown below the figures, taken at Q_{water} = 0.004, 0.05 and 0.111 μL s^{-1} for I, II and III respectively and Q_{oil} = 0.417, 0.139 and 0.019 μL s^{-1} for IV, V and VI respectively. (c) Dimensionless length of the droplets (L/w) plotted as a function of the ratio of the rates of flow of the discontinuous and continuous fluids for the reference geometry (h = 33 μm, w = 100 μm, w_{in} = 50 μm). There are five different series of data plotted on this graph, each corresponding to a different combination of the viscosity (μ) of the continuous fluid and its rate of flow (Q_{oil}). The legend is given in the figure. There is a hundred-fold difference in the shear stress $\tau \propto Q_{oil}\mu$ between curves (○) and (■).

Available models of break-up in a T-junction

Thorsen *et al.*[3] suggested that the droplets are sheared off from the stream of the discontinuous fluid and the size of the droplets is determined by the competition between the Laplace pressure $p_L \approx 2\gamma/r$, where r is the characteristic radius of curvature of the liquid–liquid interface, and the shear stress exerted on this interface by the continuous fluid. This balance led to the estimate $r \approx \gamma\varepsilon/\mu u$, where ε is the characteristic dimension of the space between the droplet and the wall of the channel and u is the mean speed of the continuous liquid through this gap. Although this estimate agreed[3] with the measured sizes of the droplets, the model was not verified rigorously: the viscosity of the carrier fluid was not changed in the experiments and thus it was not possible to distinguish between the stresses exerted as a result of the build-up of pressure upstream of the emerging droplet, and the shear stresses acting on the tip of the discontinuous fluid. Tice *et al.*[21] suggested that the change of viscosity of the continuous fluid results in a change of the ranges of rates of flow at which the system produces monodisperse droplets, but did not discuss the influence of viscosity on the size of the drops. Here, we describe experiments conducted in order to test the postulated—'shear dominated'—scaling relations. The results of these experiments have led us to conclude that the size of the droplets generated in T-junction geometries that are typically used in microfluidic experiments is not determined by a relation between the Laplace pressure and the shear stress, and to suggest an alternative scaling that we discuss below.

Effect of viscosity of the continuous phase

To characterize the role of the shear stress exerted by the continuous fluid on the interface in the break-up process we measured the length L of the droplets produced in the reference T-junction as a function of Q_{water}, at different values of Q_{oil} and μ (Fig. 2c). For any fixed value of Q_{oil} and μ there

Table 1 The dimensions of the relevant geometrical parameters for the five different T-junction devices that we tested in our experiments. We refer to geometry 1 as the reference device

Geometry	w_{in}/μm	h/μm	w/μm	h/w_{in}	w/w_{in}
1	50	33	100	2/3	2
2	50	33	50	2/3	1
3	50	33	200	2/3	4
4	100	33	100	1/3	1
5	50	79	100	~3/2	2

are two distinct regimes characterized by different scaling of L with Q_{water}: at low values of Q_{water}, L is constant, while in the second regime L grows approximately linearly with increasing Q_{water}. The system crosses over from $L \sim$ constant to $L \propto Q_{water}$ approximately at $Q_{water} = Q_{oil}$.

This behavior could be explained within the 'shearing' model: at low Q_{water} the flow of the discontinuous fluid would be much slower than the flow of the host fluid around the droplet, and therefore Q_{water} would not affect the balance between the shear stress and the interfacial tension. At large Q_{water} the shear stress exerted by the continuous liquid on the droplet would decrease simply because the difference of the speeds of the two fluids would decrease with increasing Q_{water}. However, within this model, the size of the droplet at the plateau (at low Q_{water}) would be determined by an equation of the form[3] $L = O(\gamma\varepsilon/\mu u)$ and should depend on both the rate of flow of the continuous fluid ($u = Q_{oil}/hw$) and on its viscosity.

In our experiments we varied both μ (10 and 100 mPa s) and Q_{oil} (0.00278, 0.0278 and 0.278 μL s^{-1}) and we observed that the value of L in the plateau region *does not* depend on either Q_{oil} or μ in spite of the fact that the values of the shear stress $\tau \propto \mu u$ span two orders of magnitude within the data shown in Fig. 2c. As we do not observe even approximately two orders of magnitude of a change in the size of the droplets, this observation excludes the shear stress as the primary factor in the break-up in the T-junction, and in determination of the sizes of droplets. The assertion that shear is not primarily responsible for break-up is consistent with the small values of capillary numbers $Ca = \mu u/\gamma$ calculated for the same series of data: Ca spans the range of $Ca \in (8 \times 10^{-5}, 8 \times 10^{-3})$ suggesting that interfacial tension dominates shear stress. Finally, we note that the minimum size of the droplets that we were able to form in these experiments was $L \sim w$ (Fig. 2c). This lower limit to size suggests that geometry of the device plays a significant role in the break-up process.

Order-of-magnitude discussion of forces involved in break-up

Motivated by these observations, we wished to identify the processes that contribute to the dynamics of pinch-off, and to establish the effects that are dominant. There are three different types of forces acting on the tip of the discontinuous phase during break-up: the surface tension force (F_γ), the shear-stress force (F_τ) and the force arising from the increased resistance to flow of the discontinuous fluid around the tip (F_R). We estimate the magnitudes of these forces for the geometry of the tip that is depicted in Fig. 3a. We observe this geometry in the intermediate stages of break-up—that is after the tip of the discontinuous phase has entered the main channel, and before the immiscible thread breaks—and the understanding of the balance of forces at this stage is, we believe, crucial for drawing the correct model of the break-up process.

Interfacial stresses

The surface tension force is associated with the Laplace pressure jump Δp_L across a static interface, $\Delta p_L = \gamma(r_a^{-1} + r_r^{-1})$, where r_a is the axial curvature (in the plane of the device) and r_r is the radius of the radial curvature (in the cross-section

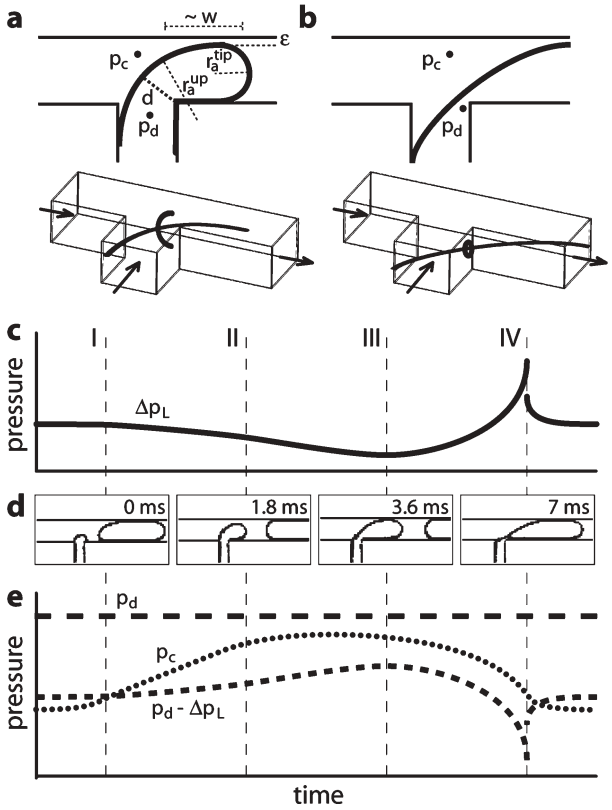

Fig. 3 (a) A schematic illustration (top view) of the shape of the tip of the immiscible thread at an intermediate stage of break-up. We denote the separation between the liquid–liquid interface and the wall of the main channel as ε. The 'length' of the tip is on the order of the width w of the main channel. The radii r_a of axial curvature (in the plane of the device) are $r_a^{tip} \sim w/2$ (at the downstream side of the tip) and $r_a^{up} \sim w$ (at the upstream side). Insets (a) and (b) show a schematic plot of the postulated evolution of pressures at the T-junction during a typical break-up process. Insets (a) and (b) illustrate the axial (in the plane of the device) and radial (in the cross-section of the neck joining the inlet for the discontinuous phase with the droplet) curvature, and the positions at which we define the hydrostatic pressures p_d and p_c in the discontinuous and continuous phases respectively. Inset (a) shows the droplet in an early stage of collapse of the neck of characteristic width d. Inset (b) shows the neck in the final phase of collapse, when the radial curvature dominates the axial curvature, and break-up occurs rapidly. We identify four stages of formation of a droplet: the stream of the discontinuous fluid enters into the main channel (I), the stream blocks the main channel (II), the droplet elongates and grows downstream (III), the droplet separates from the inlet (IV). The intervals between these stages are not uniform. (c) Evolution of the Laplace pressure jump across the interface (Δp_L), (d) micrographs of the reference system (h = 33 μm, w = 100 μm, w_{in} = 50 μm) for Q_{water} = 0.14 μL s^{-1} and Q_{oil} = 0.083 μL s^{-1}. The time lapses between consecutive micrographs and the first one are given in the figure. (e) Schematic illustration of the evolution of the hydrostatic pressure p_d in the discontinuous phase at the end of the inlet, pressure p_c in the continuous phase in the junction, and the difference $p_d - p_L$.

of the neck joining the inlet for the discontinuous fluid with the tip). In the intermediate stage of the process of formation of a droplet (Fig. 3a) the radial curvature is bounded by the height of the channels ($h < w$) and $r_r \approx h/2$ (or less) everywhere. The axial curvature is greater at the downstream tip of the

immiscible thread ($r_a^{tip} \approx w/2$) than at the upstream side of it ($r_a^{up} \approx w$): the interface on the downstream side of the thread acts on the liquid inside the thread with a stress $p_L \approx -\gamma(2/w + 2/h)$ (the minus sign signifies that the stress is oriented upstream), and the interface located upstream acts on the discontinuous liquid with a stress $p_L \approx \gamma(1/w + 2/h)$ (oriented downstream). The sum of the two, multiplied by the cross-section of the channel gives the estimate of the surface tension force $F_\gamma \approx -\gamma h$, oriented upstream, which has a *stabilizing* effect on the tip: in the absence of any other stresses or forces, surface tension would position the tip symmetrically about the axis of the inlet channel for the discontinuous phase. When the continuous fluid flows in the main channel, both the shear stress exerted by the host fluid on the droplet and the pressure drop along the axis of the main channel distort the emerging droplet in the downstream direction.

Shear stress

We can approximate[3] the shear stress exerted on the tip by the continuous phase as: $\tau \approx \mu u_{gap}/\varepsilon$ where $u_{gap} = Q_{oil}/h\varepsilon$ is the speed of the continuous fluid flowing through the gap between the interface and the wall of the channel (of characteristic thickness ε (Fig. 3a)). We estimate the net force acting on the immiscible tip by multiplying the shear stress $\tau \approx \mu Q_{oil}/h\varepsilon^2$ by the surface area of the interface in the gap $A_{gap} \sim hw$, where we take w as the characteristic axial length-scale of the tip (Fig. 3a). The corresponding net force on the tip is pointed downstream and has the magnitude of $F_\tau \approx \mu Q_{oil}(w/\varepsilon^2)$. This calculation over-estimates the shear force for two reasons. First, it assumes that the tip of the discontinuous fluid is stationary when, if fact, the dispersed fluid flows downstream. Second, it assumes that the volumetric flow of the continuous fluid around the emerging droplet is equal to the externally fixed rate of flow through the device (Q_{oil}). In reality, the flow at the T-junction is not stationary, and—as we explain in detail below—once the immiscible tip blocks the cross-section of the main duct, the continuous fluid displaces—squeezes—the neck connecting the emerging droplet with the side-inlet channel. As we only try to estimate the magnitudes of the forces acting on the immiscible tip, we do not try to take these two effects into account in the calculation, and only observe that both of them act to lower the actual shear force exerted on the emerging droplet.

Resistance to flow of the continuous fluid

The thread of the discontinuous fluid partially blocks the cross section of the main channel (Fig. 3a) and leads to an increased resistance to flow of the continuous fluid. For $\varepsilon \sim w$ we use the Hagen–Poiseuille equation to estimate the pressure drop (Δp) over the length ($\sim w$) of the immiscible tip: $\Delta p \approx \mu Q_{oil} w/h^2\varepsilon^2$. For $\varepsilon \ll w$ we estimate Δp for a thin film of typical or largest thickness ε, width h and length w (Fig. 3a): $\Delta p \approx \mu Q_{oil} w/h\varepsilon^3$, and the corresponding force $F_R \approx \Delta p h w = O(\mu Q_{oil} w^2/\varepsilon^3)$. The exact value of the exponent n to which the thickness of the film ε should be raised in the above expression can be derived from a detailed lubrication analysis[47] for flow around objects near-filling the cross-sections of capillaries: n depends on the geometry of the cross-section of the capillary and on the geometry and material parameters of the object. Importantly, n is larger than 2—*e.g.* in a circular capillary, a translating rigid sphere or a clean bubble can be described with[47] $n = 2.5$. Consequently we can expect that $F_R > F_\tau$ when $\varepsilon \ll w$.

To summarize the order-of-magnitude estimates of the forces acting on the tip, we note that the only stabilizing force arises from the surface tension effects. There are two destabilizing forces, both of which increase sharply upon the decrease of the separation ε between the interface and the wall of the main channel. In most of the geometries tested in our experiments we observe that $\varepsilon/w \ll 1$, and under such conditions, we expect that the leading contribution in the break-up dynamics is the force F_R arising from the pressure drop associated with the resistance to flow of the continuous fluid around the immiscible tip.

Postulated model of break-up

On the basis of this analysis and observation, we postulate that the dynamics of break-up in a typical T-junction (here the reference geometry 1, see Table 1), is dominated by the balance of pressures in the discontinuous (p_d) and continuous (p_c) phases at the junction. We first draw a heuristic picture of the break-up process, and propose the scaling relation arising from this model. Then we compare the predictions of this model with our experimental measurements.

We start with the analysis of the evolution of the Laplace pressure jump Δp_L exerted on the discontinuous liquid by the interface, $\Delta p_L = \gamma(r_a^{-1} + r_r^{-1})$, where r_a is the axial curvature (in the plane of the device) and r_r is the radius of the radial curvature (in the cross-section of the collapsing neck joining the inlet for the discontinuous fluid with the droplet). In the initial stage of the process of formation of the droplet, when the tip of the discontinuous phase enters the main channel, both the radial and axial curvatures are bound by the dimensions of the inlet channel (w_{in} and h). When the tip enters the main channel and grows in the downstream direction, the shape of the interface of the upstream side of the neck joining the droplet with the inlet evolves with time. After the discontinuous phase fully enters the main channel, the neck has a characteristic width d (Fig. 3a). Over time this neck thins and finally breaks. The axial curvature of the neck is smaller than that of the initial axial curvature of the tip of the discontinuous fluid. The radial curvature of the neck is at first (when $d > h$) bound by height of the channel $r_r < h/2$. When $d < h$, the neck assumes a circular cross-section of radius r_r and the radial curvature grows (Fig. 3b).

We identify four stages of the process of formation of a droplet (Fig. 3c and d): (I) the tip of the discontinuous phase enters the main channel, (II) the growing droplet spans the whole cross-section of the main channel ($\varepsilon \ll w$), (III) the droplet elongates in the downstream direction and the neck connecting it to the inlet thins (d decreases), and (IV) the neck breaks, the disconnected droplet flows downstream and the tip of the discontinuous phase recoils back towards the inlet. Between the first and second stage the Laplace pressure decreases (because the radial curvature is still bound by the height of the channel and the axial curvature of the interface located upstream of the tip decreases); this process continues

until stage III, when $d \approx h$, and the radial curvature starts to grow. The Laplace pressure reaches a maximum value at the moment of break-up (as the radial curvature grows to infinity), and after pinch-off p_L relaxes back to the initial value.

Pressures in the discontinuous and continuous fluids during break-up

A detailed model of break-up in the T-junction would consider the total normal stress on the interface. In the region near the droplet where there are thin films, the stresses are dominated by the pressure contribution and thus we limit our discussion to the analysis of the evolution of pressures in the discontinuous (p_d) and continuous (p_c) fluid at the junction during the process of the formation of a droplet. Since we are only interested in the difference of these two pressures, for simplicity we assume that the pressure in the discontinuous fluid at the end of its inlet remains constant throughout the break-up process (long-dashed line in Fig. 3e). The net pressure exerted by the discontinuous fluid on the host liquid ($p_d - p_L$) is shown with a short dashed line. In stage one (I) the tip of the discontinuous phase penetrates into the main channel, hence $p_d - p_L > p_c$. In stages II, III and IV, the value of p_c increases as a consequence of the increased resistance to flow of the continuous fluid through the thin films of characteristic thickness ε. In stage II, ε acquires its minimum value ($\varepsilon \ll w$), and consequently p_c is now greater than $p_d - p_L$ and the upstream side of the interface of the tip starts to travel downstream. In stage four the neck of the immiscible thread breaks, the tip recoils to the inlet channel for the discontinuous phase and the pressure in the continuous phase drops to its unperturbed value.

Proposed scaling relation for the size of the droplets

On the basis of the above model of the evolution of pressures at the T-junction during break-up, we draw the following quantitative prediction for the size of the droplet. First the tip of the discontinuous phase enters and blocks the main channel. At this moment the 'length' of the droplet is approximately equal to the width of the channel. The increased pressure in the continuous fluid upstream of the immiscible thread starts to 'squeeze' the neck (of characteristic width d (see Fig. 3a)). The thickness of the neck decreases at a rate which is approximately equal to the mean speed of flow of the continuous fluid: $u_{squeeze} \approx u = Q_{oil}/hw$. During this process the drop elongates at rate $u_{growth} \approx Q_{water}/hw$. The final length of the drop is therefore equal to: $L \approx w + (d/u_{squeeze})u_{growth} = w + dQ_{water}/Q_{oil}$. It is convenient to non-dimensionalize this equation to: $L/w = 1 + \alpha(Q_{water}/Q_{oil})$, with $\alpha = (d/w)$, which recovers eqn (1). Since some of the flow of the continuous fluid bypasses the droplet and does not contribute to squeezing, and as the speed at which the neck collapses need not be constant, *etc*., it is reasonable to treat α as a fitting parameter of order one.

The two terms—the constant and the ratio of the rates of flow—in the scaling of the size of the droplets can be understood as follows. The time t to form the droplet is the sum of the time it takes to fill the cross-section of the main channel ($t_{fill} \propto 1/Q_{water}$) and the time to squeeze the neck connecting the inlet channel with the emerging droplet ($t_{squeeze} \propto 1/Q_{oil}$). The size of the droplet can be estimated as the product of t and Q_{water}. When the rate of flow of the continuous fluid is much greater than the rate of flow of the dispersed phase ($Q_{water}/Q_{oil} \ll 1$), $t \approx t_{fill}$ and the size of the droplet is constant ($L/w \approx t_{fill}Q_{water} \approx 1$) simply because once the droplet fills the cross-section of the channel it is broken-off quickly ($t_{squeeze} \ll t_{fill}$). In this regime, the size of the droplets does not depend on the particular values of either of the rates of flow. When ($Q_{water}/Q_{oil} > 1$) $t \approx t_{squeeze}$ and the dominant contribution to the size of the droplet arises from the inflow of the discontinuous fluid into the droplet during the squeezing stage, and thus $L/w \propto t_{squeeze}Q_{water} \approx Q_{water}/Q_{oil}$. In this regime, the size of the droplets depends crucially on the particular values of each of the rates of flow.

Verification of the scaling effect of viscosity, interfacial tension and the geometry of the junction

Fig. 4 shows a comparison of the predicted (for $\alpha = 1$) and measured lengths of droplets formed in our reference T-junction geometry for a wide range of rates of flow of both phases and for two different viscosities of the continuous fluid. In spite of its simplicity, the model agrees well with the experimental data. We also tested the dependence of the length of the droplets on the rates of flow of the fluids in four different geometries (Table 1), and the model predicts the size well for all of the series (see ESI†). The experiments in which the width of the main channel (w = 200 μm) was much greater

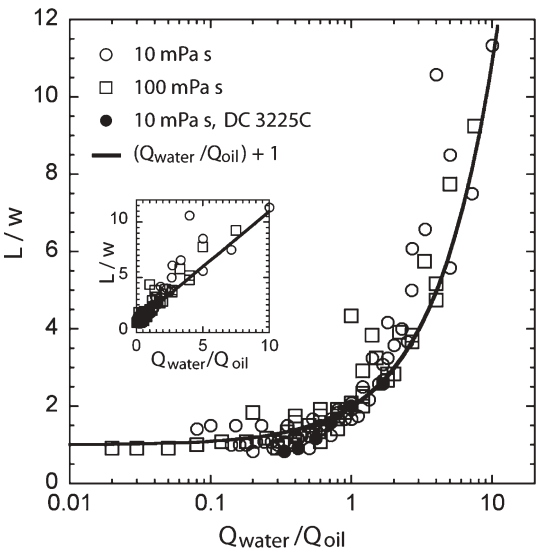

Fig. 4 Comparison of the measured lengths L of the droplets with the prediction of the simple model derived from the postulated mechanism of break-up for two different viscosities μ of the continuous fluid (μ = 10 mPa s (○, ●), and μ = 100 mPa s (□)). The series denoted with (●) was obtained for the continuous fluid containing surfactant DC3225C (1% w/w, Dow Corning). The rates of flow span the following ranges (in μL s^{-1}): $Q_{water} \in (2 \times 10^{-3}, 0.5)$ and $Q_{oil} \in (0.014, 0.556)$ for μ = 10 mPa s, and $Q_{water} \in (5 \times 10^{-4}, 0.389)$ and $Q_{oil} \in (0.0014, 0.278)$ for μ = 100 mPa s. We conducted all these experiments in the reference geometry of the T-junction (h = 33 μm, w = 100 μm, w_{in} = 50 μm). The solid line gives the postulated scaling $L/w = 1 + Q_{water}/Q_{oil}$. The inset represents the same graph on a linear scale.

than the width w_{in} of the inlet channel (w/w_{in} = 4), demonstrated the effects of the shear stress exerted on the liquid–liquid interface (see ESI†). In these experiments the droplets did not fill the cross-section of the main channel before they break off from the inlet, and the viscosity of the continuous fluid changed the observed lengths of the droplets in a systematic way (see Fig. S2 of ESI†).

The transition from squeezing ($\varepsilon/w \ll 1$) to shearing ($\varepsilon \sim w$) may be estimated simply: if the typical length-scale l^* at which the shear stress is exactly balanced by the Laplace pressure $l^* \approx \gamma w/\mu u$ is greater than the width w of the outlet channel, then the emerging drop does not yield to shear exerted by the continuous fluid and effectively blocks the channel. Under these circumstances the squeezing mechanism is expected to describe the break-up. When $l^*/w < 1$, shear stress becomes sufficiently important to affect the sizes of the droplets produced. In practice, however, we observe that the ratio of the width of the inlet channel to the width of the main channel is a very important parameter in this transition. For the same capillary numbers we observe that when $w_{in}/w \geqslant 1/2$, the droplets break in the 'squeezing' mode (the tip of the immiscible thread blocks the whole cross-section of the main channel), and our model correctly predicts the size of the droplets. For $w_{in}/w < 1/2$ we observe that the shear stress exerted on the immiscible tip distorts the drop significantly and the squeezing model and the scaling proposed in this article no longer apply. Detailed analysis of the deformation of a droplet adhering to a wall and subject to simple shear flow—as a function of the ratio of the size of the droplet to the area of attachment, and various other parameters—can be found elsewhere.[48–50]

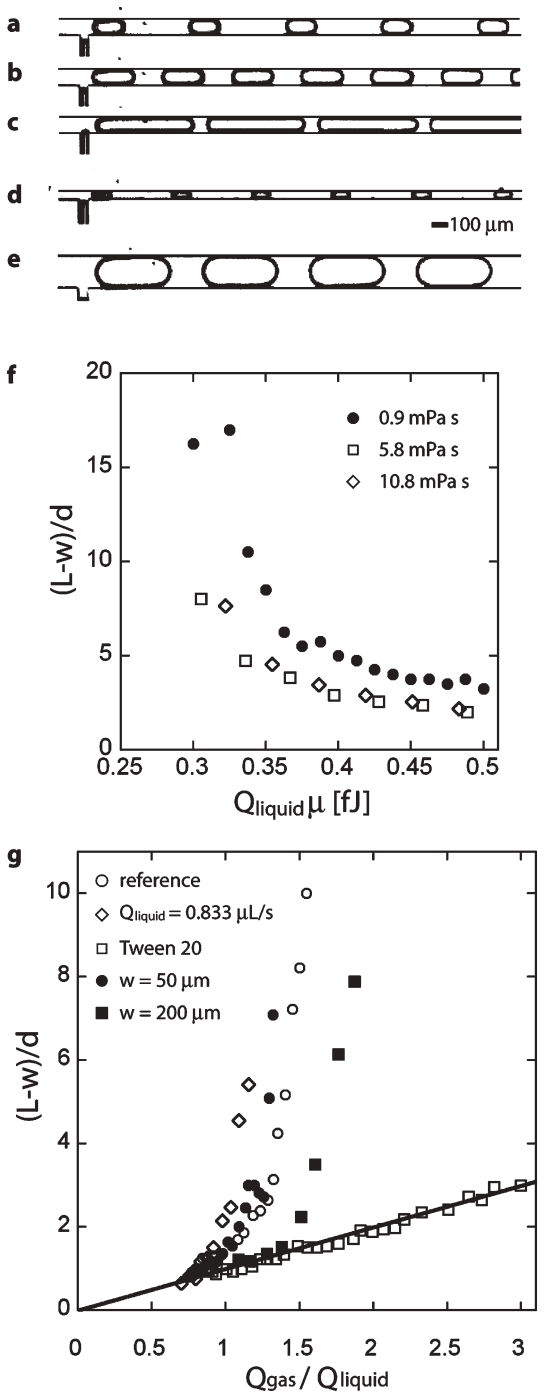

Fig. 5 Optical micrographs of bubbles of nitrogen in a surfactant-free aqueous flow produced with a microfluidic T-junction device. (a)–(c) Depict the reference geometry (100 μm-wide outlet channel) for a constant rate of flow of water (0.417 μL s^{-1}) and with the pressure of the gas set at 34.3 kPa (a), 41.9 kPa (b) and 49.0 kPa (c). Inset (d) depicts a system with a 50 μm-wide outlet channel at the same rate of flow of water and with the pressure of nitrogen set at 83.9 kPa, while (e) shows a system with a 200 μm-wide outlet channel at the same rate of flow of water and with the pressure of nitrogen set at 21.2 kPa. (f) The length of the bubbles produced in the reference T-junction as a function of the factor ($Q_{liquid}\mu$) of the rate of flow of the continuous fluid and its viscosity for three different viscosities (see legend in the figure) and for fixed pressure applied to the gas stream p = 41 kPa. (g) Scaling of the length of the bubbles produced in T-junction geometries. Q_{gas} is calculated according to $Q_{gas} = p/R$, where R gives the estimate of the viscous resistance to flow in the outlet channel (L_{ch} = 2 cm for all the curves)—see text. (○) Reference geometry (h = 33 μm, w = 100 μm, w_{in} = 50 μm) at Q_{liquid} = 0.417 μL s^{-1}; (◇) same geometry, Q_{liquid} = 0.833 μL s^{-1}; (□) same geometry, Q_{liquid} = 0.417 μL s^{-1}, continuous liquid containing surfactant Tween 20 (2% w/w); (●) and (■) w = 50 and 200 μm respectively, Q_{liquid} = 0.417 μL s^{-1}. The solid line gives the predicted scaling $(L - w)/d = Q_{gas}/Q_{liquid}$. The fitting parameter d = 50 μm for all the curves besides the one for w = 200 μm, for which d = 100 μm.

3. Gas–liquid systems

The pressure drop Δp that is needed to drive the continuous fluid around the immiscible thread does not depend critically on the viscosity of the dispersed fluid. Both in the case of a viscous droplet and in the case of a gaseous bubble, which block the flow of the carrier fluid, Δp increases sharply upon decrease of the thickness ε of the film separating the interface from the walls of the channel. Thus the mechanism of break-up that we described for liquid–liquid systems should apply equally well to liquid–gas systems (Fig. 5a–e). The length L of the bubbles produced in a T-junction should follow the same scaling: $L = d(Q_{gas}/Q_{liquid}) + w$, where Q_{gas} is the rate of inflow of gas into the main channel given by $Q_{gas} = p/R$, where R is the resistance to flow in this channel and p is the difference in pressures between the inlet of the gas and the outlet of the main channel, located the length L_{ch} downstream from the

T-junction. For low volume-fractions of bubbles in the downstream portion of the main channel, to a first order approximation, we can assume that the R will scale as it would in a channel filled with the continuous liquid: $R \propto \mu L_{ch}/h^2w^2$.

Verification of proposed scaling

To test the postulated scaling, we made three checks: (i) the effect of viscosity of the continuous liquid on the length of the bubbles, (ii) the effect of the length of the outlet channel and (iii) the effect of the geometrical parameters of the T-junction.

According to the postulated scaling, the length of the bubbles should be inversely proportional to the viscosity of the continuous liquid, since $(L - w)/d = Q_{gas}/Q_{liquid} = p/Q_{liquid}R \propto p/(Q_{liquid}\mu)$ (because $R \propto \mu$). In Fig. 5f, we plot $(L - w)/d$ as a function of $(Q_{liquid}\mu)$ for p = 41 kPa and for three different viscosities of the liquid (μ = 0.9, 5.8 and 10.8 mPa s). The curves are similar in shape and magnitude, this observation supports the prediction that $(L - w)/d$ scales inversely with μ. In order to check further that the length of the bubbles produced in the T-junction is inversely proportional to the viscous resistance to flow in the outlet channel, we change the length L_{ch} of this channel by incorporating 'resistors'—10 cm long sections of the outlet channel. According to the squeezing model, $(L - w)/d = Q_{gas}/Q_{liquid} = p/Q_{liquid}R \propto p/L_{ch}$ (because $R \propto \mu$) and hence $[(L - w)/d]L_{ch} \propto p$. Experiments with networks containing one (n = 1) and two (n = 2) resistors confirm this scaling (see Fig. S2 of ESI†)—a twofold increase of the resistance of the outlet channel caused a twofold decrease of the size of the bubbles.

Finally, we compare the lengths of bubbles formed in T-junctions characterized by different widths of the main channel. In Fig. 5g, we plot $(L - w)/d$ as a function of the ratio Q_{gas}/Q_{liquid} for three different geometries (w = 50, 100 and 200 μm). The lengths of the bubbles observed in experiment agree with the predicted scaling (shown with the solid line in Fig. 5g) for small bubbles and small volume fractions of bubbles in the outlet channel. At larger lengths of bubbles and larger volume fractions, the length of the bubbles increases much more rapidly with the increase of the applied pressure than the model predicts. We speculate that the origin of this discrepancy is that the model overestimates the resistance to flow in the outlet channel at high volume fraction of the gaseous phase: as the volume fraction of the bubbles in the outlet channel grows, the ratio of the actual resistance to flow in the outlet channel to the resistance estimated for the clean continuous fluid drops substantially. This drop results in larger rate of flow of gas, than that predicted in our simple model, and larger sizes of bubbles. Surprisingly, when the liquid contained surfactant, the lengths of the bubbles followed our simple model almost ideally (Fig. 5g). Decoration of the gas–liquid interface with surfactant has a pronounced influence on the resistance to flow of the liquid and bubbles in the outlet channel. When the interface is clean (free of surfactants) the continuous fluid confined to the thin films between the gas–liquid interface and the walls of the channels is stationary.[51,52] Then, the dissipation occurs only in the liquid in between the bubbles, and because there is less liquid between the bubbles than if the channel was filled with liquid only, the resistance is smaller. In contrast, an interface decorated with surfactant supports the shear stress, and the liquid adjacent to the interface flows at the speed of the bubble. The motion of the fluid in the thin films adds to the resistance to flow, and—surprisingly—in the experiment that we performed it resulted in a resistance very similar (judging by the applicability of our model) to the resistance of the continuous fluid flowing at the same superficial speed. In order to generalize this observation, however, this result should be tested over a wider range of types and concentrations of surfactants.

4. Conclusions

We have demonstrated that under conditions that are typical for use of the microfluidic T-junction (widths and heights on the order of 10 to 100 μm and rates of flow on the order of 0.01 to 1 μL s^{-1}), and for small values of the capillary number the dominant effect in the break-up of either liquid or gaseous streams in the continuous fluid is the balance of hydrostatic pressures in the two immiscible fluids. The 'squeezing' mechanism of break-up is specific to microsystems as it depends crucially on the blockage of the channel by a liquid or gaseous plug. This mechanism allows formulation of a simple scaling law that predicts the size of droplets and bubbles produced in microfluidic T-junctions. We find that the geometries that promote the squeezing mechanism can be described by two conditions: (i) the width of the main channel should be greater than its height, and (ii) the width of the inlet channel should be at least equal to half the width of the main channel.

We note that in the survey presented in this paper we explored only systems in which the viscosity of the dispersed phase is smaller than the viscosity of the continuous phase. It is an interesting question if—and how—an increased viscosity of the dispersed phase will modify the scaling relations presented herein.

Results of numerical simulations[22] for a T-junction in which $w = w_{in} = h$, confirm the mechanism of break-up that we postulated here including the evolution of pressures in the continuous and discontinuous phases depicted schematically in Fig. 3. These simulations show that there is a transition from the squeezing (pressure-dominated) to dripping (shear-dominated) mechanism of break-up at a value of the capillary number of the order of 10^{-2}.

The squeezing mechanism of break-up, particular to low values of capillary numbers and confined geometries of microfluidic systems, implies two important experimental predictions: (i) it should be possible to form emulsions at very small length-scales (when $Ca \ll 1$), and (ii) it is possible to form not only liquid droplets but also bubbles, regardless of whether the interface is saturated with surfactants or not. The increased pressure drop along a droplet that fills the cross-section of the channel can be expected in channels with cross-sections different than rectangular, *e.g.* circular, and thus the squeezing regime of break-up should also be observed in such geometries.

The quantitative model presented in this survey should facilitate tuning the architecture of the T-junction and

choosing the rates of flow resulting in sizes of the droplets required for specific applications.

5. Experimental procedures

Preparation of the microfluidic devices

We fabricated the devices using photolithography and soft lithography.[53] We used a transparency mask to produce a photoresist master that we then covered in polydimethylsiloxane (PDMS). After the PDMS cured, we sealed the slab containing the channels in relief to either a flat slab of PDMS (for the droplet-generating systems) or a glass microscope slide (for the bubble-generating systems). The PDMS slabs and glass slides were exposed to an oxygen plasma prior to sealing.[54] We placed the droplet-generating systems in an oven at 100 °C for 24 h so that the surface of the PDMS would become uniformly hydrophobic prior to use. The bubble-generating systems, on the other hand, were used immediately after sealing to ensure that the surface of the PDMS remained hydrophilic.

Fluids

We performed two sets of experiments: in the first one we dispersed water (Milipore, viscosity μ_{water} = 0.9 mPa s at 24 °C) in silicon oil (Fluka, viscosity μ = 10 mPa s, and 100 mPa s). In some experiments the continuous (oil) phase contained an emulsifier (DC 3225C, Dow Corning, 2% w/w). The interfacial tension between the silicone oil and water was $\sim$36.5 mN m^{-1} without the surfactant.[55] We forced both liquids into the system at externally fixed rate of flow (Q_{water} and Q_{oil}) with digitally operated syringe pumps (Harvard Apparatus, PhD2000) through PET tubing (PE60, Intramedic). In the second set of experiments we dispersed gas (nitrogen) in aqueous solutions of glycerol (μ = 0.9, 5.8 and 11 mPa s for 0%, 52% and 62% glycerol w/w). In some experiments water contained Tween 20 surfactant (Fluka, 2% w/w). In the case of pure water–nitrogen interface we assume the value of interfacial tension γ to be the same as for a water–air interface (γ = 72 mN m^{-1}). Addition of Tween 20 (2% w/w) lowers this value to ($\gamma \approx$ 35 mN m^{-1}). Here we control the pressure p applied to the gas stream and the rate of flow Q_{water} of the aqueous solutions.

After changing any of the flow parameters (rates of flow or pressure), we waited an appropriate amount of time before taking measurements to let the system relax to a steady-state flow (in the inlet channels) and a stable break-up process. This relaxation time depended largely on the rates of flow of the fluids flowing through the system. At high rates ($\sim$1–10 μL s^{-1}) equilibration was fast—on the order of few seconds. At the lowest rates of flow (10^{-4}–10^{-2} μL s^{-1}) the system required several (1 to 30) minutes for the system to become stable. In practice, after changing any of the rates of flow, we waited until the systems started to produce uniform series of droplets (or bubbles), added and additional time (1 to 10 min) to ensure equilibration, and than proceeded with the measurements.

Observation and image analysis

We visualized the behavior of the system through a microscope. We used a high-speed camera (Phantom V7) to record movies of the formation of bubbles and droplets, and measured their sizes (lengths) using Adobe Photoshop.

Acknowledgements

P.G. thanks the Foundation for Polish Science for a postdoctoral fellowship and H.A.S. thanks Unilever Research for support. We thank A. Colin and colleagues for helpful conversations. This work was supported by the U.S. Department of Energy under award DE-FG02-OOER45852. Additional salary support was provided by the National Institutes of Health (NIGMS) under award GM065364. We thank the Harvard MRSEC (DMR-0213805) for the use of micro-fabrication facilities and fast cameras.

References

1 K. Hosokawa, T. Fujii and I. Endo, *Anal. Chem.*, 1999, **71**, 4781–4785.
2 S. Sugiura, M. Nakajima, S. Iwamoto and M. Seki, *Langmuir*, 2001, **17**, 5562–5566.
3 T. Thorsen, R. W. Roberts, F. H. Arnold and S. R. Quake, *Phys. Rev. Lett.*, 2001, **86**, 4163–4166.
4 S. L. Anna, N. Bontoux and H. A. Stone, *Appl. Phys. Lett.*, 2003, **82**, 364–366.
5 J. D. Tice, H. Song, A. D. Lyon and R. F. Ismagilov, *Langmuir*, 2003, **19**, 9127–9133.
6 D. R. Link, S. L. Anna, D. A. Weitz and H. A. Stone, *Phys. Rev. Lett.*, 2004, 92.
7 H. J. Liu, M. Nakajima and T. Kimura, *J. Am. Oil Chem. Soc.*, 2004, **81**, 705–711.
8 S. Okushima, T. Nisisako, T. Torii and T. Higuchi, *Langmuir*, 2004, **20**, 9905–9908.
9 C. P. Steinert, I. Goutier, O. Gutmann, H. Sandmaier, M. Daub, B. de Heij and R. Zengerle, *Sens. Actuators, A*, 2004, **116**, 171–177.
10 Q. Y. Xu and M. Nakajima, *Appl. Phys. Lett.*, 2004, **85**, 3726–3728.
11 I. Kobayashi, X. F. Lou, S. Mukataka and M. Nakajima, *J. Am. Oil Chem. Soc.*, 2005, **82**, 65–71.
12 S. Takeuchi, P. Garstecki, D. B. Weibel and G. M. Whitesides, *Adv. Mater.*, 2005, **17**, 1067.
13 A. M. Ganan-Calvo, *Phys. Rev. E*, 2004, 69.
14 A. M. Ganan-Calvo and J. M. Gordillo, *Phys. Rev. Lett.*, 2001, 87.
15 P. Garstecki, I. Gitlin, W. Diluzio, E. Kumacheva, H. A. Stone and G. M. Whitesides, *Appl. Phys. Lett.*, 2004, **85**, 2649–2651.
16 P. Garstecki, H. A. Stone and G. M. Whitesides, *Phys. Rev. Lett.*, 2005, **94**, 164501.
17 T. Cubaud and C. M. Ho, *Phys. Fluids*, 2004, **16**, 4575–4585.
18 J. M. Gordillo, Z. D. Cheng, A. M. Ganan-Calvo, M. Marquez and D. A. Weitz, *Phys. Fluids*, 2004, **16**, 2828–2834.
19 A. Gunther, S. A. Khan, M. Thalmann, F. Trachsel and K. F. Jensen, *Lab Chip*, 2004, **4**, 278–286.
20 B. Zheng and R. F. Ismagilov, *Angew. Chem., Int. Ed.*, 2005, **44**, 2520–2523.
21 J. D. Tice, A. D. Lyon and R. F. Ismagilov, *Anal. Chim. Acta*, 2004, **507**, 73–77.
22 M. De Menech, P. Garstecki, F. Jousse and H. A. Stone, *Transition from squeezing to dripping in a microfluidic T-shaped junction*, in preparation.
23 P. B. Umbanhowar, V. Prasad and D. A. Weitz, *Langmuir*, 2000, **16**, 347–351.
24 C. Cramer, P. Fischer and E. Windhab, *Chem. Eng. Sci.*, 2004, **59**, 3045–3058.
25 P. J. A. Kenis, R. F. Ismagilov and G. M. Whitesides, *Science*, 1999, **285**, 83.
26 H. A. Stone, A. D. Stroock and A. Ajdari, *Annu. Rev. Fluid Mech.*, 2004, **36**, 381–411.

27 J. W. Hong and S. R. Quake, *Nat. Biotechnol.*, 2003, **21**, 1179–1183.
28 S. K. W. Dertinger, X. Y. Jiang, Z. Y. Li, V. N. Murthy and G. M. Whitesides, *Proc. Natl. Acad. Sci. U. S. A.*, 2002, **99**, 12542.
29 E. M. Luchetta, J. H. Lee, L. A. Fu, N. H. Patel and R. F. Ismagilov, *Nature*, 2005, **434**, 1134–1138.
30 T. A. Thorsen, *Biotechniques*, 2004, **36**, 197–199.
31 S. K. Sia, V. Linder, B. A. Parviz, A. Siegel and G. M. Whitesides, *Angew. Chem., Int. Ed.*, 2004, **43**, 498–502.
32 M. Y. He, J. S. Edgar, G. D. M. Jeffries, R. M. Lorenz, J. P. Shelby and D. T. Chiu, *Anal. Chem.*, 2005, **77**, 1539–1544.
33 Y. C. Tan, J. S. Fisher, A. I. Lee, V. Cristini and A. P. Lee, *Lab Chip*, 2004, **4**, 292–298.
34 S. K. Cho, H. J. Moon and C. J. Kim, *J. Membr. Sci.*, 2003, **12**, 70–80.
35 B. Zheng, J. D. Tice and R. F. Ismagilov, *Adv. Mater.*, 2004, **16**, 1365–1368.
36 V. Srinivasan, V. K. Pamula and R. B. Fair, *Lab Chip*, 2004, **4**, 310–315.
37 S. Q. Xu, Z. H. Nie, M. Seo, P. Lewis, E. Kumacheva, H. A. Stone, P. Garstecki, D. B. Weibel, I. Gitlin and G. M. Whitesides, *Angew. Chem., Int. Ed.*, 2005, **44**, 724–728.
38 D. Dendukuri, K. Tsoi, T. A. Hatton and P. S. Doyle, *Langmuir*, 2005, **21**, 2113–2116.
39 W. J. Jeong, J. Y. Kim, J. Choo, E. K. Lee, C. S. Han, D. J. Beebe, G. H. Seong and S. H. Lee, *Langmuir*, 2005, **21**, 3738–3741.
40 W. J. Jeong, J. Y. Kim, S. Kim, S. H. Lee, G. Mensing and D. J. Beebe, *Lab Chip*, 2004, **4**, 576–580.
41 M. Seo, Z. Nie, S. Xu, P. Lewis and E. Kumacheva, *Langmuir*, 2005, **21**, 4773–4775.
42 D. Rudhardt, A. Fernandez-Nieves, D. R. Link and D. A. Weitz, *Appl. Phys. Lett.*, 2003, **82**, 2610–2612.
43 J. Su, M. R. Bringer, R. F. Ismagilov and M. Mrksich, *J. Am. Chem. Soc.*, 2005, **127**, 7280–7281.
44 B. Zheng, J. D. Tice, L. S. Roach and R. F. Ismagilov, *Angew. Chem., Int. Ed.*, 2004, **43**, 2508–2511.
45 H. Song and R. F. Ismagilov, *J. Am. Chem. Soc.*, 2003, **125**, 14613–14619.
46 T. Ward, M. Faivre, M. Abkarian and H. A. Stone, *Electrophoresis*, 2005, **26**, 3716–3724.
47 H. A. Stone, *Chem. Eng. Sci.*, 2005, **60**, 4838–4845.
48 A. D. Schleizer and R. T. Bonnecaze, *J. Fluid Mech.*, 1998, **383**, 29–54.
49 X. F. Li and C. Pozrikidis, *J. Fluid Mech.*, 1996, **307**, 167–190.
50 S. Yon and C. Pozrikidis, *Phys. Fluids*, 1999, **11**, 1297–1308.
51 G. I. Taylor, *J. Fluid Mech.*, 1961, **10**, 161.
52 H. Wong, C. J. Radke and S. Morris, *J. Fluid Mech.*, 1995, **292**, 71.
53 D. C. Duffy, J. C. McDonald, O. J. A. Schueller and G. M. Whitesides, *Anal. Chem.*, 1998, **70**, 4974–4984.
54 J. C. McDonald, D. C. Duffy, J. R. Anderson, D. T. Chiu, H. Wu, O. J. A. Schueller and G. M. Whitesides, *Electrophoresis*, 2000, **21**, 27–40.
55 P. Erni, P. Fischer and E. Windhab, *Ann. Trans. Nor. Rheo. Soc.*, 2004, **12**, 175.

